Int. J. Electrochem. Sci., 15 **(2020)** 11779 – 11790, doi: 10.20964/2020.12.18

International Journal of
ELECTROCHEMICAL
SCIENCE
www.electrochemsci.org

Study on Microbial Corrosion Resistance of Ni-P-Ag Coatings in Artificial Marine Environments Containing Sulphate-reducing Bacteria

Dazhang Yang[1,2,3], *Naixin Wang*[1,2], *Jing Xie*[1,3,*], *Jinfeng Wang*[1,4]

[1] College of Food Science & Technology, Shanghai Ocean University, Shanghai 201306, China.
[2] Shanghai Professional Technology Service Platform on Cold Chain Equipment Performance and Energy Saving Testing Evaluation, Shanghai 201306, China
[3] Quality Supervision, Inspection, and Testing Center for Cold Storage and Refrigeration Equipment, Ministry of Agriculture， Shanghai 201306, China
[4] National Experimental Teaching Demonstration Center for Food Science and Engineering (Shanghai Ocean University), Shanghai 201306, China
[*]E-mail: jxie@shou.edu.cn

Received: 10 August 2020/ *Accepted:* 21 September 2020/ *Published:* 31 October 2020

In this paper, silver was electroless-plated onto nickel-phosphorus (Ni-P) to improve its microbial corrosion resistance. The microbial corrosion behaviour of nickel-phosphorus-silver (Ni-P-Ag) in artificial marine environments with *Desulfovibrio desulfuricans* was experimentally investigated. Fluorescence microscopy (FM), scanning electron microscopy (SEM), and X-ray fluorescence (XRF) were used to analyse the colonization of sulphate-reducing bacteria (SRB). The results indicate that Ni-P-Ag could not inhibit the growth of SRB, which were still able to proliferate wihin a short period. Based on the electrochemical impedance spectroscopy (EIS) results, the potentiodynamic curves of Ni-P-Ag were concentrated from 1 d to 31 d with almost no shift in the negative direction. The corrosion potentials and lgI_{corr} of the Ni-P-Ag potentiodynamic curves changed slowly. The Nyquist and Bode plots of Ni-P-Ag coating in seawater containing SRB were both relatively stable. According to the equivalent circuits, the R_{ct} of Ni-P-Ag decreased slowly from 5.75 kΩ·cm^{-2} to 2.35 kΩ·cm^{-2}. The results showed that the microbial corrosion resistance of silver coating is obvious. Although silver coating could not inhibit SRB reproduction, Ni-P-Ag can effectively resist SRB corrosion.

Keywords: Sulphate-reducing bacteria, Microbial corrosion, Silver, Seawater

1. INTRODUCTION

Microbial corrosion is an important problem in the energy, marine, and oil industries [1, 2]. Some bacteria can accelerate the corrosion of metals and alloys, even if they are corrosion-resistant [3-

6]. Microbial corrosion of alloys and metals can be divided into two categories: chemical and electro-microbial influenced corrosion. Sulphate-reducing bacteria (SRB) are common bacteria that are widespread in soil and water environments. Rao et al. [7] pointed out that the amount of SRB in seawater cooling system during fouling is 10^5-10^6 cfu·g^{-1}. Wang et al. [8] investigated the fouling process of stainless steel tube heat exchangers using three species of bacteria: iron bacteria (IB), SRB, and slime-forming bacteria (HB). They found that SRB generally undergo biofouling fastest in stainless steel. Consequently, SRB in seawater was used to microbially corrode metal in this paper.

Over the past few years, materials have incorporated new technology to improve the corrosion and stain resistance of equipment, such as electroless plating [9-11]. Electroless-plated nickel (EN) with a Ni-P alloy coating was used to improve the wear resistance and corrosion resistance of the material due to its high hardness and wear resistance. [12-18]. However, the antibacterial performance of Ni-P is unsatisfactory. In a previous study, it was found that SRB can accelerate the deterioration of Ni-P in marine environments [5]. SRB and their metabolites convert the oxides of nickel to sulphides, which form a surface passivation film that must be broken down. Michalska et al. [19] also found that the resistance of SRB-covered Ni-Ti alloys decrease, with higher capacitance in the barrier region of the oxide. In addition, fouled Ni-P may lose its abrasion resistance due to its surface properties, which tend to significantly deteriorate after each fouling run [20].

Silver was used to improve the antimicrobial corrosion in this paper. As a kind of broad-spectrum antibacterial, silver can inhibit microbial growth [21]. According to some studies, silver or its nanoparticles inhibit SRB reproduction. El-Salam et al. [22] found that Ag nanoparticles (AgNPs) with poly(2-aminothiophenol) (P2ATH) and poly(2-methylaniline) enhance the efficiencies of anti-sulphate-reducing bacteria. Omran et al. [23] investigated the biocidal activity of silver nanoparticles (AgNPs) against halotolerant SRB. The results showed that the biocidal activity of mycosynthesized AgNPs against halotolerant planktonic SRB makes it an attractive option to control microbial corrosion. However, some studies reveal the opposite conclusion. For instance, Chen et al. [24] investigated the effect of AgNPs on SRB. They found that AgNPs stimulate the proliferation of D. vulgaris rather than exerting inhibitory or biocidal effects.

This paper investigates the microbial corrosion of Ni-P-Ag coatings by SRB, where the corrosion resistance of silver has been separately verified. Ni-P-Ag corrosion experiments were carried out in media containing SRB and compared with Ni-P. The morphology of SRB colonies on the Ni-P surface was observed by FM and SEM analysis. XRF analysis was used to infer the corrosion products. To study the corrosion behaviour, electrochemical experiments were carried out. In addition, equivalent circuits were used to visualize the microbial corrosion behaviour and estimate Ni-P-Ag corrosion.

2. EXPERIMENTS AND METHODS

2.1. Ni-P-Ag and Ni-P electroless plating

Brass was used as the substrates for electroless plating, and the synthesis was carried out in two steps. First, electroless nickel plating was carried out. $NiSO_4 \cdot 6H_2O$ (30.0 g·l^{-1}), $NaH_2PO_2 \cdot H_2O$ (36.0

$g \cdot l^{-1}$), and CH_3COONa (15.0 $g \cdot l^{-1}$) were used as the main reagents [25]. One group of Ni-P was used as a control group. The substratea were degreased 5 minutes with acetone and alkaline rinsing with a 10 mass% NaOH solution, then pickling 1 minute with 10 vol% HCl solution for 1 minute and activating with 5 vol% HCl solution. The Ni-P electroless plating was completed after 2 hours in 90-95 ° C water bath. The other group of samples was plated with silver by using Tollens' reagent, which was made by a silver ion solution and a reducing agent solution [26]. The silver ion solution and reducing agent solution were prepared separately. The silver ion solution contained $AgNO_3$ (3.0 $g \cdot L^{-1}$), NaOH (2.1 $g \cdot L^{-1}$), and NH_3H_2O (60 $ml \cdot L^{-1}$). The reducing agent solution contained $C_6H_{12}O_6$ (2.25 $g \cdot L^{-1}$), $C_4H_6O_6$ (0.2 $g \cdot L^{-1}$) and C_2H_5OH (5 $ml \cdot L^{-1}$). The silver ion solution and reducing agent solution were mixed just before plating. The electroless plating silver was completed after 30 minutes at 20-25 ° C.

2.2. Microbial corrosion experiment

In the corrosion experiments, the slices were hung vertically in a closed test tube containing a bacterial suspension, which was placed in a thermostat cabinet at 30 °C. Samples of Ni-P-Ag and Ni-P were placed in SRB suspension for 31 days and 28 days, respectively. To maintain the biological activity of SRB, the bacterial suspension in the test tube was replaced every 72 hours, and the replacement bacterial suspension was incubated for 36 hours. *Desulfovibrio vulgaris* (ATCC 7757) was used in our experiments. Modified Baar's Medium (ATCC Medium 1249) was used as the culture medium for sulphate reduction. The medium must be autoclaved at 121 °C to sterilize and remove as much oxygen as possible. *Desulfovibrio vulgaris* was cultured in anaerobic bottles with Medium 1249 at 30 °C. Based on the optical density determined by a microplate reader (iMark^{TM}), SRB colonization reaches a stable stage after culturing for 36 hours, and transformation of the culture medium into a bacterial suspension can then be used in microbial corrosion experiments.

Approximately every 7 days, a group of slices was taken for electrochemical analysis. As shown in Figure 1 a), the coupons were hung in a breaker with artificial seawater. The 1000 mL artificial seawater consisted of 27.43 g sodium chloride, 3.38 g magnesium sulphate, 2.34 g magnesium chloride, 1.14 g calcium chloride, and 0.76 g potassium chloride. The front and back sides of the sample were covered with silicone, as shown in Figure 1 b). Therefore, only a 10 mm x 10 mm area of seawater was exposed during the experiment. A CHENHUA CHI660E Electrochemical Workstation (China) was used for the electrochemical impedance spectroscopy, with a sinusoidal AC excitation signal amplitude of 10 mV and a scanning frequency range of 10^{-2}-10^5 Hz. A three-electrode cell was used with coupons, a platinum electrode, a saturated calomel electrode (SCE) as the working electrode, the counter electrode, and the reference electrode, respectively. The potentiodynamic polarization curves were also drawn by the CHENHUA CHI660E Electrochemical Workstation.

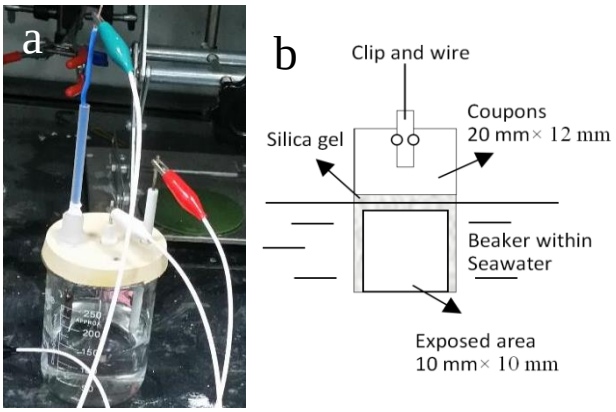

Figure 1. Experimental setup for the electrochemical analysis a) Photograph of the experimental beaker with a three-electrode cell b) Diagram of the hanging slice.

2.3. Morphology analysis

Morphological studies of SRB on specimens were performed by FM and SEM analysis. After the coupons were washed with deionized water and placed in 100 mg·L-1 acridine orange solution for 15 minutes, they were observed by fluorescence microscopy (NIKON Ti-E). The excitation and emission wavelengths of acridine orange are 502 nm and 526 nm, respectively. In addition, the surfaces of the coupons were observed using a scanning electron microscope (Hitachi SU70). The potentiodynamic polarization test was conducted using a scan rate of 0.167 mV s^{-1}. The EIS test was operated at the open circuit potential, with a voltage perturbation amplitude of 10 mV in a frequency range of 10^5 Hz to 10 mHz. In addition, XFR analysis was used to investigate the composition on the specimen surface using a wavelength dispersive X-ray fluorescence spectrometer (Shimadzu XRF-1800).

3. RESULTS AND DISCUSSION

3.1. Morphology analysis of SRB biofilm

FM results showed rapid colonization of SRB on Ni-P-Ag surfaces. As shown in Figure 2, the induction period for the discovery of SRB is usually less than 2 days. Little SRB was found after 1 d, but after 2 d, SRB rapidly multiplied and covered the surface of the specimen. The SRB then aggregated to appear clumpy after 5 d, as shown in Figure 2 (c). This means that the anti-corrosion of silver has little effect on the colonization of SRB. Chen et al. also found that silver nanoparticles stimulated the proliferation of SRB rather than exerting inhibitory or biocidal effects [24].

Figure 3 shows SEM images of the specimen when the coupons were immersed in SRB suspension for 0 d and 31 d, respectively. In Figures 3 (a) and (b), particulate matter densely covered the specimen, which was composed of the corrosion products and EPS (extracellular polymeric substance). The EPS could acidify the solution and accelerate alloy corrosion [28]. To investigate the corrosion on the coupon surface, XRF analysis was performed to compare the composition of corrosion products in the experimental groups.

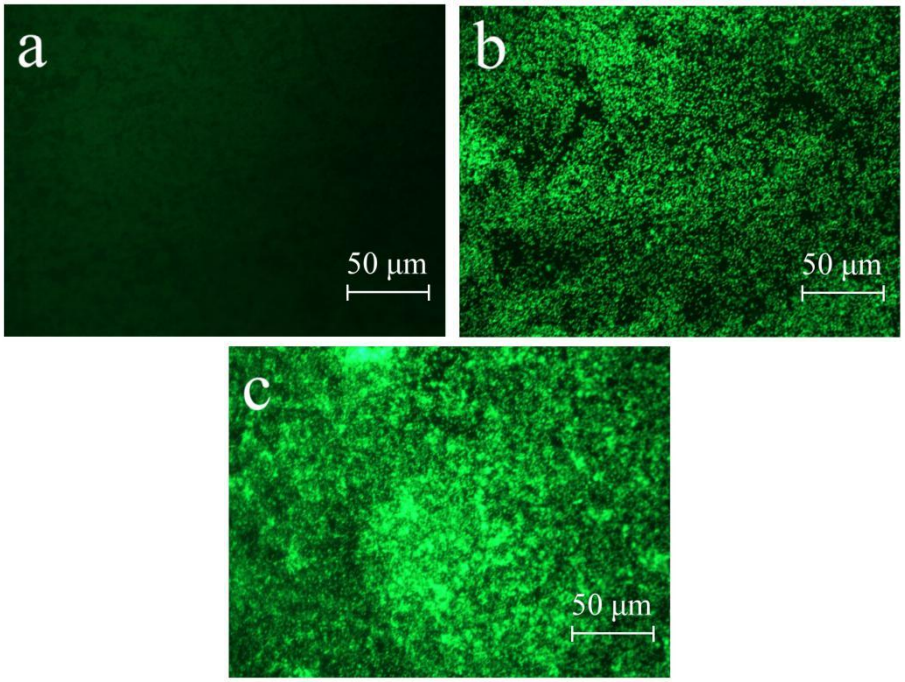

Figure 2. Fluorescence images of Ni-P-Ag surface SRB (exposure was 200 ms): (a) 1 d, (b) 2 d, and (c) 5 d.

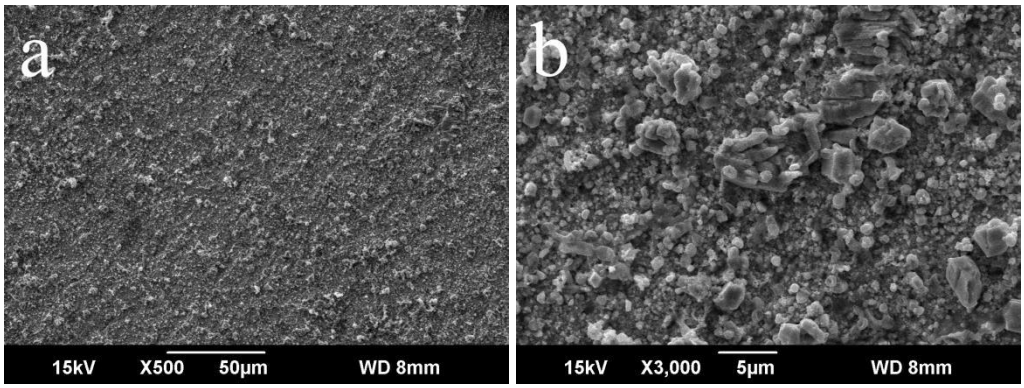

Figure 3. Representative SEM images of the Ni-P-Ag surface containing SRB (a) 31 d at 50 μm and (b) 31 d at 5 μm.

Table 1. Comparison of the composition of coupons in the experimental group by XRF analysis

Elements	0 d	10 d	31 d
Ag	98.9	93.1	90.7
C	1.02	1.59	1.56
S	0.0216	0.731	2.44
Si	0.0169	0.0243	0.0321
O	0	3.16	3.85
N	0	1.14	1.129
Fe	0	0.113	0.226
P	0	0.023	0.0264
Others	0	0.129	0.0093

Due to the electroless silver coating, the mass percent of silver was 98.9%, as shown in Table 1. A general conclusion is that SRB reduces SO_4^{2-} to H_2S and that EPS has sulphide [1, 2, 28, 29]. When metals are exposed to SRB, sulphides are the primary corrosives [30-33]. Compared with the coupons after immersion in SRB suspension 31 d, the mass percent of O is only 3.85%, and S is only 2.44%.

In our previous study, S and O on the Ni-P surface immersed in SRB suspension for 28 d were as high as 19.39% and 8.93%, respectively [5]. It follows that the silver on the surface of Ni-P-Ag showed effective corrosion resistance.

3.2. Polarization curves

Figure 4 shows the Ni-P-Ag potentiodynamic curves after immersion in SRB suspension. The potentiodynamic curves were concentrated, and the corrosion potential barely moves in the negative direction after 7 d in the Ni-P-Ag group. The results showed that the corrosion rate of Ni-P-Ag was low and stable. In contrast, the cathode and anode branches of the Ni-P group were changed. The corrosion potential moves in the negative direction, and the corrosion current increases from 7 d to 28 d. This implies increased anodic depolarization and accelerated corrosion due to the destruction of the oxide film on the Ni-P surface. Hamilton et al. [34] found that SRB makes it possible to degrade the protective film. This leads to an active corrosion cell between the sulphide film (cathode) and the nearby metal substrate (anode), accelerating its corrosion rate. It does not occur in the Ni-P-Ag group, which means that Ni-P-Ag has good corrosion resistance to SRB.

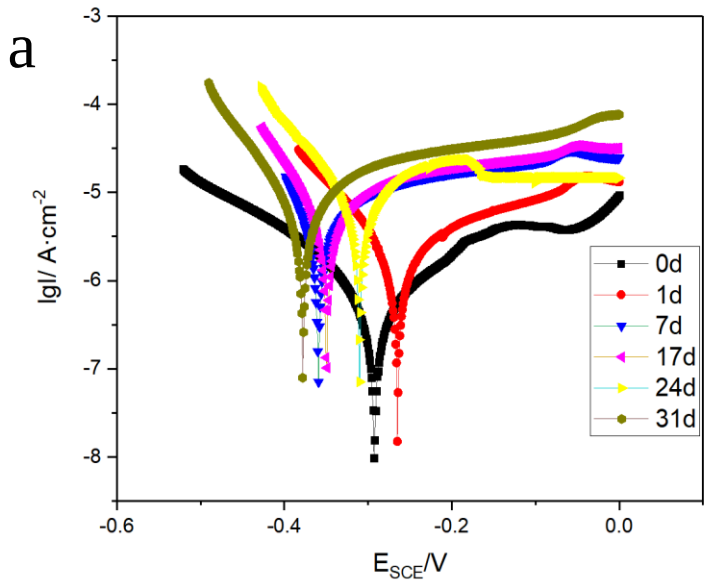

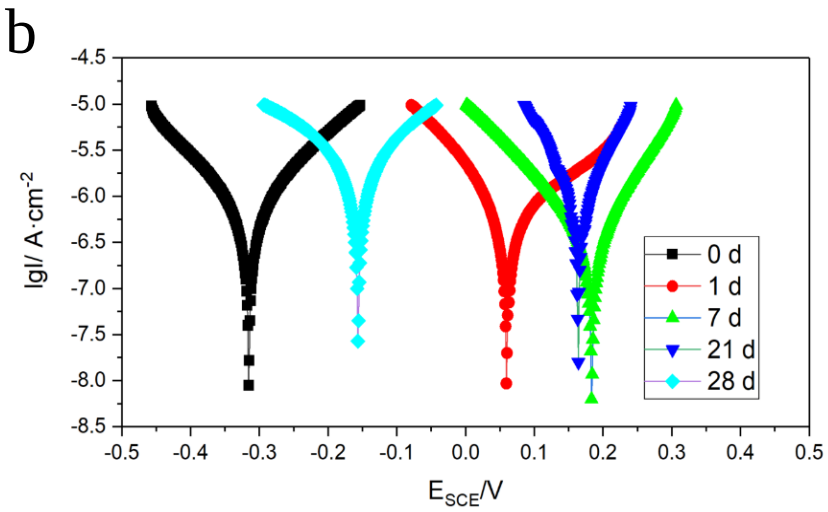

Figure 4. Polarization curves of Ni-P-Ag coating (a) and Ni-P coating (b) in artificial seawater containing SRB for different corrosion times. Scan rate: 0.167 mV s^{-1}

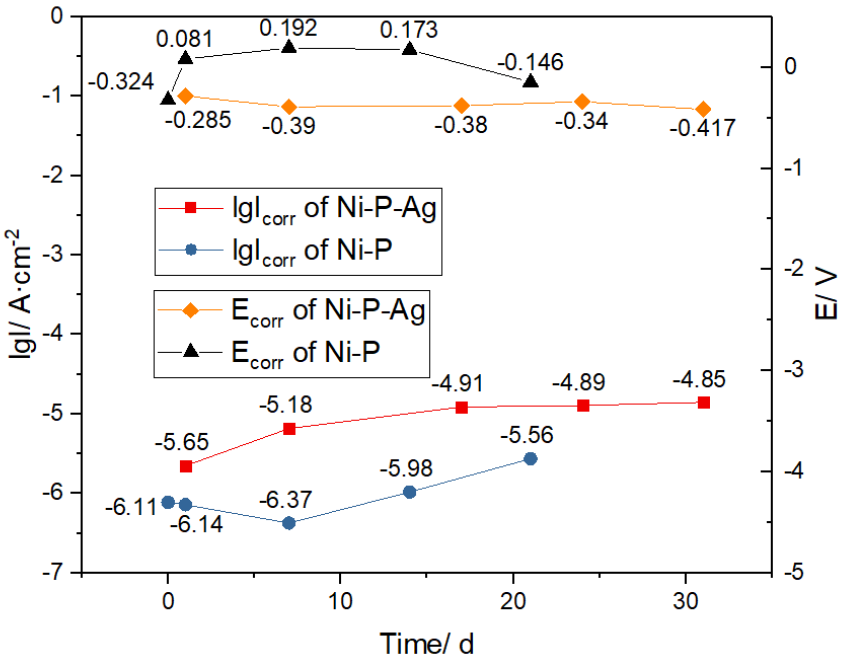

Figure 5. The I_{corr} and E_{corr} of Ni-P-Ag coating and Ni-P coating in artificial seawater containing SRB for different corrosion times.

Additionally, the lgI_{corr} and E_{corr} of graphite epitaxy were inferred from the potentiodynamic curves of Ni-P-Ag and Ni-P, as seen in Figure 5. The lgI_{corr} of Ni-P in the SRB suspension increased from -6.37 A·cm^{-2} to -5.56 A·cm^{-2} after 7 d, and E_{corr} decreased from 0.192 V to -0.146 V after 7 d. In the Ni-P-Ag group, lgI_{corr} and E_{corr} were relatively stable. lgI_{corr} changed from between -4.85 A·cm^{-2} to -5.65 A·$cm^{-2,}$ and E_{corr} was changed between -0.285 V to -0.417 V. This means that the corrosion rate of Ni-P-Ag is stable and less affected by SRB than Ni-P.

3.2. Electrochemical impedance spectroscopy of Ni-P-Ag coating samples

Figure 6(a) shows the Nyquist and Bode plots of Ni-P-Ag coatings in SRB suspensions from 1 to 31 d. From 1 to 31 d, the curving direction of the Nyquist lines changed anticlockwise to clockwise. Figure 6(b) shows the Bode diagram of the Ni-P-Ag coating in the SRB suspension for 1-31 d. At low frequencies, lg|*Z*| decreased with time. In contrast, lg|*Z*| increased with time from 1 to 31 d at high frequency, which is due to microbial corrosion by SRB. However, the Nyquist diagram of the Ni-P-Ag coating is almost linear, and the difference in the Bode diagram is quite small. This means that the corrosion of Ni-P-Ag is not serious.

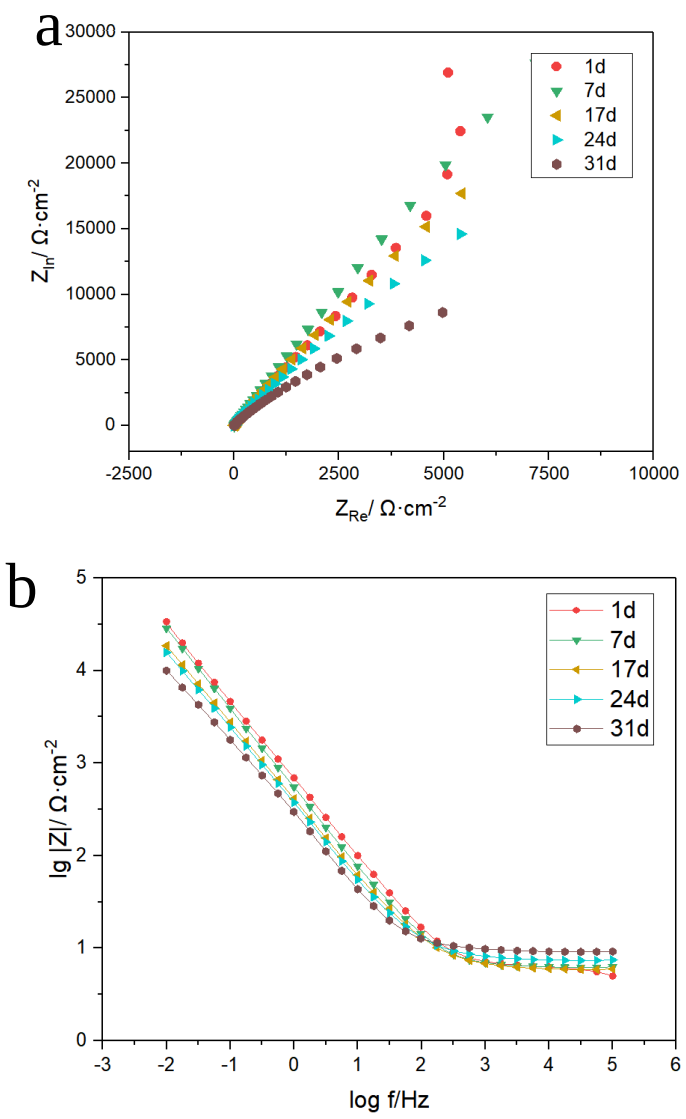

Figure 6. Nyquist plots (a) and Bode plots (b) of Ni-P-Ag coating in artificial seawater containing SRB for different corrosion times. Sinusoidal AC excitation signal amplitude: 10 mV, frequency range: 10^{5}~10^{-2} Hz.

The equivalent circuit for the microbial corrosion of Ni-P-Ag coatings in SRB suspensions using ZsimWin 3.60 software is shown in Figure 7. In Figure 7, the resistance of the electrolyte

solution, passive film, charge transfer, and capacitance of the passive film and double layer are denoted as R_s, R_{pf}, R_{ct}, C_{pf}, and C_{dl}, respectively. The results show that the Nyquist plot fitting of Ni-P-Ag coatings in SRB suspensions was successful by using a two-layer equivalent circuit and two layers in series. The oxide film is in the upper layer, and the surface impedance is in the lower layer. Resistors and capacitors are connected in parallel to form the impedance of the oxide film. [35].

/

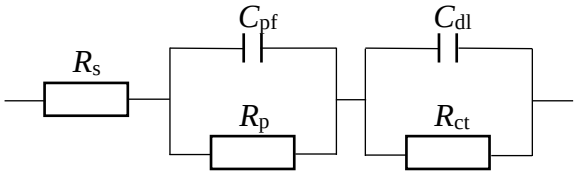

Figure 7. Equivalent circuit for fitting EIS data to Ni-P-Ag coating in artificial seawater containing SRB

The fitted values of the equivalent circuit are shown in Table 2, where C_{dl} can be described as $Z_c=Y_o^{-1}(j\omega)^{-n}$ ($0<n<1$) [36]. C_{pf} is a constant phase angle element (CPE) explained by the sample's surface roughness and the heterogeneous biofilm dispersion effect [37]. Since R_{ct} is much larger than other resistors, R_{ct} is typically used to evaluate the corrosion rate [36]. The fitting values of R_{ct} of Ni-P-Ag are relatively stable, as shown in Table 2, which decreased from 5.75 $k\Omega \cdot cm^{-2}$ to 2.35 $k\Omega \cdot cm^{-2}$. Sulphide deposited on the surface disrupts a portion of the passivation film and promotes the cathodic polarization process in the crevice, thereby increasing the electron transfer rate [36, 38]. In comparison, the R_{ct} of Ni-P under the same experimental conditions changed from 80.6 $k\Omega \cdot cm^{-2}$ to 22.4 $k\Omega \cdot cm^{-2}$. It was concluded that the corrosion was low on the surface of Ni-P-Ag according to the R_{ct}. This means that silver coating is helpful for the anti-corrosion of Ni-P.

Table 2. Fitted values of EIS to equivalent circuits (1 d to 31 d)

Time (day)	parameter	fitted value	error (%)
1	R_s ($\Omega \cdot cm^{-2}$)	3.29E+00 $\Omega \cdot cm^{-2}$	4.998
	C_{pf} (F)	6.14E-07 F	11.93
	R_{pf} ($\Omega \cdot cm^{-2}$)	2.94E+00 $\Omega \cdot cm^{-2}$	5.274
	C_{dl}-Y_o	3.18E-04	0.4806
	C_{dl}-n	8.37E-01	0.1486
	R_{ct} ($\Omega \cdot cm^{-2}$)	5.75E+03 $\Omega \cdot cm^{-2}$	13.87
7	R_s ($\Omega \cdot cm^{-2}$)	6.23E+00 $\Omega \cdot cm^{-2}$	0.6254
	C_{pf} (F)	1.03E-03 F	16.45
	R_{pf} ($\Omega \cdot cm^{-2}$)	7.68E+05 $\Omega \cdot cm^{-2}$	18.1
	C_{dl}-Y_o	5.93E-04	8.062
	C_{dl}-n	7.98E-01	1.175
	R_{ct} ($\Omega \cdot cm^{-2}$)	5.82E+04 $\Omega \cdot cm^{-2}$	10.72
17	R_s ($\Omega \cdot cm^{-2}$)	5.96E+00 $\Omega \cdot cm^{-2}$	0.709
	C_{pf} (F)	9.56E-04 F	9.647

24	R_{pf} ($\Omega \cdot cm^{-2}$)	1.30E+05 $\Omega \cdot cm^{-2}$	36.94
	C_{dl}-Y_o	1.04E-03	6.273
	C_{dl}-n	7.40E-01	1.006
	R_{ct} ($\Omega \cdot cm^{-2}$)	5.84E+03 $\Omega \cdot cm^{-2}$	17.8
	R_s ($\Omega \cdot cm^{-2}$)	7.50E+00 $\Omega \cdot cm^{-2}$	0.5415
	C_{pf} (F)	1.12E-03 F	5.183
	R_{pf} ($\Omega \cdot cm^{-2}$)	7.84E+04 $\Omega \cdot cm^{-2}$	18.15
	C_{dl}-Y_o	1.07E-03	3.067
	C_{dl}-n	7.61E-01	0.5239
	R_{ct} ($\Omega \cdot cm^{-2}$)	4.24E+03 $\Omega \cdot cm^{-2}$	10.99
31	R_s ($\Omega \cdot cm^{-2}$)	9.35E+00 $\Omega \cdot cm^{-2}$	0.5612
	C_{pf} (F)	1.64E-03 F	3.737
	R_{pf} ($\Omega \cdot cm^{-2}$)	2.53E+04 $\Omega \cdot cm^{-2}$	7.571
	C_{dl}-Y_o	1.19E-03	1.905
	C_{dl}-n	7.94E-01	0.4641
	R_{ct} ($\Omega \cdot cm^{-2}$)	2.35E+03 $\Omega \cdot cm^{-2}$	10.81

4. CONCLUSIONS

To study the microbial corrosion effects of SRB on Ni-P-Ag coating, experimental procedures were performed in this paper. The colonization of SRB on the Ni-P-Ag surface was analysed by FM, SEM, and XRF. The experimental results show that Ni-P-Ag cannot inhibit SRB growth and will proliferate in a short period of time.

Based on the EIS analysis, the experimental data of Ni-P-Ag coating was compared with that of Ni-P coating. The potentiodynamic curve profile of Ni-P-Ag was concentrated and stable in the negative direction from 1 d to 30 d. The corrosion potentials and lgI_{corr} of the Ni-P-Ag potentiodynamic curves changed slowly. In contrast, the corrosion potential of the potentiodynamic curves of Ni-P shifted significantly in the negative direction, with a dramatic increase in the lgI_{corr} of Ni-P. This means that SRB corrode more slowly in Ni-P-Ag in seawater compared to Ni-P.

Both the Nyquist and Bode plots of Ni-P-Ag coatings in seawater containing SRB showed little change. The diameters of the Nyquist plot diameters were so large that the data were nearly linear, but the curving direction of the Nyquist lines changed from anticlockwise to clockwise. The corrosion resistance of Ni-P-Ag was proven by the equivalent circuits. The fitting values of R_{ct} of Ni-P-Ag decreased from 5.75 $k\Omega \cdot cm^{-2}$ to 2.35 $k\Omega \cdot cm^{-2}$.

In conclusion, although silver coating could not inhibit SRB reproduction, the corrosion rate of Ni-P-Ag is low and is less affected by SRB than Ni-P. Accordingly, it was concluded that the microbial corrosion resistance of silver coating is effective.

DISCLOSURE STATEMENT

There are no conflicts to declare.

FUNDING
This paper is supported by the “Chen Guang” project supported by the Shanghai Municipal Education Commission and Shanghai Education Development Foundation (16CG55) and the Public Service Platform Construction Project of Shanghai Science and Technology Commission (17DZ2293400).
ORCID Dazhang Yang https://orcid.org/0000-0001-7742-2963

References

1. M. Wu, T. Wang, K. Wu, L. Kan, *Constr. Build. Mater.*, 239 (2020) 117813.
2. R. Jia, T. Unsal, D. Xu, Y. Lekbach, T. Gu, *Int. Biodeter. Biodegr.*, 137 (2019) 42.
3. Jie Sun, Xiaodong Zhao, Husong Rong, Shiyu Yang, Shuai Wang, Zhongyi An, Yan Li, Xinlei Qu, *Int. J. Electrochem. Sci.*, 15 (2020) 2364.
4. D. Yang, Y. Lei, J. Xie, Z. Shu, X. Zheng, *Mater. Technol.*, (2019) 1.
5. D. Yang, J. Liu, X. E, L. Jiang, Ann. Nucl. *Energy*, 94 (2016) 767.
6. M. Izadi, D.K. Aidun, P. Marzocca, H. Lee, *Appl. Therm. Eng.*, 31 (2011) 2464.
7. T. S. Rao, A. J. Kora, P. Chandramohan, B. S. Panigrahi, S. V. Narasimhan, *Biofouling*, 25 (2009) 581.
8. D. Wang, C. Qian, S. Cao, Y. Liu, J. Sun, Advanced Materials Research, 724-725 (2013) 1282.
9. J. A. Barish, J. M. Goddard, *Food Bioprod. Process.*, 91 (2013) 352.
10. J. Michalska, M. Sowa, R. P. Socha, W. Simka, B. Cwalina, *Electrochim. Acta*, 249 (2017) 135.
11. P. Rajala, M. Bomberg, E. Huttunen-Saarivirta, O. Priha, M. Tausa, L. Carpén, *Materials*, 9 (2016) 475.
12. A. S. Hamdy, M. A. Shoeib, H. Hady, O. F. A. Salam, *J. Appl. Electrochem.*, 38 (2008) 385.
13. S. Afroukhteh, C. Dehghanian, M. Emamy, *Progress in Natural Science: Materials International*, 22 (2012) 318.
14. V. K. Bulasara, H. Thakuria, R. Uppaluri, M. K. Purkait, *Desalination*, 268 (2011) 195.
15. H. R. Molla, H. Modarress, M. Abdouss, *Journal of Coatings Technology and Research*, 9 (2012) 183.
16. B. Ma, R. Wang, *Metals*, 8 (2018) 328.
17. M. Hao, M. Xiao, Y. Yan, Y. Miao, *Adv. Powder Technol.*, 28 (2017) 3095.
18. Z. Sharifalhoseini, M. H. Entezari, R. Jalal, *Surface and Coatings Technology*, 266 (2015) 160.
19. C. A. González-Rodríguez, F. J. Rodríguez-Gómez, J. Genescá-Llongueras, *Electrochim. Acta*, 54 (2008) 86.
20. A. Al-Janabi, M. R. Malayeri, H. Müller-Steinhagen, *Int. J. Therm. Sci.*, 49 (2010) 1063.
21. C. L. Arnaout, C. K. Gunsch, *Environ. Sci. Technol.*, 46 (2012) 5387.
22. H. M. A. El-Salam, E. M. S. Azzam, R. S. Aboad, *Int. J. Polym. Mater. Po.*, 67 (2018) 501.
23. B. A. Omran, H. N. Nassar, S. A. Younis, N. A. Fatthallah, A. Hamdy, E. H. El-Shatoury, N. S. El-Gendy, *J. Appl. Microbiol.*, 126 (2019) 138.
24. Z. Chen, J. Lu, S. Gao, M. Jin, P. L. Bond, P. Yang, Z. Yuan, J. Guo, *Water Res.*, 129 (2018) 163.
25. J. Tian, X. Liu, J. Wang, X. Wang, Y. Yin, *Mater. Chem. Phys.*, 124 (2010) 751.
26. Q. Zhao, Y. Liu, C. Wang, *Appl. Surf. Sci.*, 252 (2005) 1620.
27. R. Guo, C. McGoverin, S. Swift, F. Vanholsbeeck, *Anal. Bioanal. Chem.*, 409 (2017) 3959.
28. B. Yin, Y. Yin, Y. Lei, L. Dong, Y. Zhang, *Chem. Phys. Lett.*, 509 (2011) 192.
29. D. Enning, J. Garrelfs, *Appl. Environ. Microb.*, 80 (2014) 1226.
30. F. M. AlAbbas, C. Williamson, S. M. Bhola, J. R. Spear, D. L. Olson, B. Mishra, A. E. Kakpovbia, *Int. Biodeter. Biodegr.*, 78 (2013) 34.
31. CG. Chen, C. R. Clayton, *J. Electrochem. Soc.*, 145 (1998) 1914.
32. M. Diez-Ercilla, J. Sánchez-España, I. Yusta, K. Wendt-Potthoff, M. Koschorreck, *Biogeochemistry*, 121 (2014) 519.

33. F. M. AlAbbas, B. Rahul, J. R. Spear, D. L. Olson, B. Mishra, *Int. J. Electrochem. Sci.*, 8 (2013) 859.
34. W. A. Hamilton, *Biofouling*, 19 (2003) 65.
35. M. E. Orazem, B. Tribollet, Time-Constant Dispersion, Electrochemical Impedance Spectroscopy, (2017)John Wiley & Sons.
36. S. Hong, Y. Wu, W. Gao, J. Zhang, Y. Zheng, Y. Zheng, *Int. J. Refract. Metals Hard Mater.*, 74 (2018) 7.
37. K. F. Khaled, M. N. H. Hamed, K. M. Abdel-Azim, N. S. Abdelshafi, *J. Solid State Electrochem.*, 15 (2011) 663.
38. X. Chen, G. Wang, F. Gao, Y. Wang, C. He, *Corros. Sci.*, 101 (2015) 1.